DTU Library

Array diagnostics, spatial resolution, and filtering of undesired radiation with the 3D reconstruction algorithm

Cappellin, C.; Pivnenko, Sergey; Jørgensen, E.; Meincke, P.

Link back to DTU Orbit

ARRAY DIAGNOSTICS, SPATIAL RESOLUTION, AND FILTERING OF UNDESIRED RADIATION WITH THE 3D RECONSTRUCTION ALGORITHM

C. Cappellin(1), S. Pivnenko(2), E. Jørgensen(1), P. Meincke(1)

(1)TICRA, Lædestræde 34, 1201 Copenhagen, Denmark, Email:cc@ticra.com,ej@ticra.com,pme@ticra.com
(2)Department of Electrical Engineering, Technical University of Denmark, Ørsteds Plads, building 348, 2800 Kgs. Lyngby, Email:sp@elektro.dtu.dk

ABSTRACT

This paper focuses on three important features of the 3D reconstruction algorithm of DIATOOL: the identification of array elements improper functioning and failure, the obtainable spatial resolution of the reconstructed fields and currents, and the filtering of undesired radiation and scattering to obtain a more accurate measured field. Results obtained by real measured data are presented.

Special attention is given to the computational advantages given by the higher-order Method of Moments-based formulation of DIATOOL. Guidelines on the recommended measurement sampling and measured field truncation for achieving the best possible reconstruction results are also provided.

1. INTRODUCTION

Accurate and general antenna diagnostics techniques to identify from the radiated measured field the electrical and mechanical errors affecting the antenna under test are of high importance for the antenna measurements community. Microwave holography, based on the well-established relation between the antenna far-field and the visible region of the plane wave spectrum [1], has been widely used for this purpose. The algorithm is general, simple and computationally very fast but has a limit in the spatial resolution of the computed extreme near-field, since the invisible region of the plane wave spectrum is always neglected. The technique presented in [2] allows the reconstruction of part of the invisible region of the plane wave spectrum, thus providing higher resolution in the computed extreme near-field, but shows some limitation when dealing with large antennas and typical measurement noise.

To overcome these limits, a new class of antenna diagnostics algorithm was developed in the last decade [3]-[9]. All algorithms are based on a 3D integral data equation relating the measured field with a set of unknown equivalent electric and magnetic currents located on a closed surface conformal to the antenna. If the a priori information that the field radiated by the unknown equivalent current is zero inside the reconstruction surface is enforced as boundary condition, the unknown equivalent currents coincide with the physical currents one would measure on the reconstruction surface, [6]-[9]. A discrete set of equations is obtained by using a standard Method of Moments discretization. It is noted that the 3D formulation described above is an inverse source problem, which is challenging and inherently ill-posed, meaning that small variations on the measured field produce large variations on the reconstructed currents. Although more demanding in terms of memory usage and computation time as compared to microwave holography, these 3D reconstruction methods allow one to reconstruct the field on an arbitrary 3D surface and give the possibility to study and solve traditional antenna diagnostics problems in a new and more accurate way. The 3D reconstruction algorithm developed by TICRA in [8]-[9] is implemented in the commercial software DIATOOL, which is today the only stand-alone antenna diagnostics product on the market.

The 3D reconstruction algorithms referenced above present some differences in the discretization scheme, the enforcement of the a-priori information and the regularization method. The discretization adopted by DIATOOL is based on higher order basis functions and higher order geometry modelling, which provide a smooth description of the currents and geometry and a far smaller number of unknowns, relative to traditional RWG functions on flat triangular faces [3]-[7]. The boundary condition is enforced on the actual surface of reconstruction by means of a quasi-Galerkin testing scheme which require fewer test functions than the point matching procedure, and avoids the need of finding an inward offset surface [6]-[7]. Finally, a generalized TSVD regularization scheme is embedded in DIATOOL, by which the a-priory knowledge of the boundary condition is used independently from the data equation. This allows one to weight the two set of integral equations differently, depending on the noise of the measurement data. Thanks to these three main differences, DIATOOL provides higher accuracy and stronger robustness against noise relative to the other methods.

There are three important antenna diagnostics applications where the 3D reconstruction is superior to traditional microwave holography, namely the identification of array elements improper functioning and failure, the obtainable spatial resolution of the reconstructed fields and currents, and the filtering of undesired radiation and scattering.

The purpose of this paper is to show the accuracy and capabilities of the 3D reconstruction algorithm of DIATOOL relative to array diagnostics, obtainable resolution and filtering of undesired radiation. Guidelines on the measurement sampling and measured field truncation for achieving the best possible reconstruction results will also be provided.

The paper is organized as follows: Section 2 summarizes the main features of the 3D reconstruction algorithm of DIATOOL, Section 3 describes an example of array diagnostics with considerations on the obtainable spatial resolution, while Section 4 focuses on filtering of undesired radiation. Conclusions are finally drawn in Section 5.

2. THE 3D RECONSTRUCTION ALGORITHM

The higher-order inverse Method of Moments algorithm implemented in DIATOOL [8]-[9] computes the tangential electric and magnetic fields $\bar{E}, \bar{H}$ on the reconstruction surface S enclosing an antenna, based on the field measured at discrete points outside the surface. The tangential fields on the reconstruction surface S are obtained by the equivalent electric and magnetic surface current densities $\bar{J}s$ and $\bar{M}s$ according to

$$\bar{J}s = \hat{n} \times \bar{H}, \tag{1}$$

$$\bar{M}s = -\hat{n} \times \bar{E} \tag{2}$$

with $\hat{n}$ being the outward normal unit vector. These equivalent currents correspond to Love's equivalence principle, since they produce zero field inside S, and are found by solving the so-called data equation, which relates the measured data and the unknown surface current densities,

$$\bar{E}^{meas}(\bar{r}) = -\eta_0 L \bar{J}s + K \bar{M}s, \tag{3}$$

where η_0 is the free space impedance and L and K are integral operators defined in [8]. The a priori information that the fields radiated by the surface current densities must be zero inside S is then enforced as a boundary condition equation [8]

$$-\eta_0 \hat{n} \times L \bar{J}_s + \left(\hat{n} \times K + \frac{1}{2} \right) \bar{M}_s = 0 \tag{4}$$

$$-\left(\hat{n} \times K + \frac{1}{2} \right) \bar{J}_s - \frac{1}{\eta_0} \hat{n} \times L \bar{M}_S = 0 \tag{5}$$

and the correct set of equivalent surface current densities is finally found. The surface of reconstruction is discretized using curvilinear patches of up to fourth order, see Figure 1.
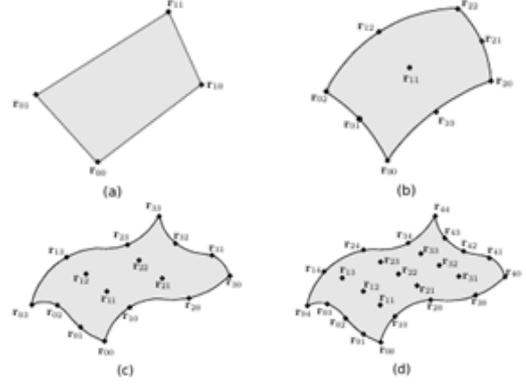

Figure 1- Curvilinear patches described by 4, 9, 16 and 25 nodes.

The electric and magnetic surface currents on each patch are expanded in higher order Legendre basis functions

$$\bar{X} = \sum_{m=0}^{M^u} \sum_{n=0}^{M^v-1} a_{mn}^u \bar{B}_{mn}^u + \sum_{m=0}^{M^v} \sum_{n=0}^{M^u-1} a_{mn}^v \bar{B}_{mn}^v, \tag{6}$$

where $\bar{X} = [\bar{J}s, \bar{M}s]$, a_{mn}^u and a_{mn}^v are unknown coefficients, M^u and M^v are the expansion orders along the u- and v- directions, and $\bar{B}_{mn}^u$ and $\bar{B}_{mn}^v$ are the u- and v-directed higher-order Legendre basis functions defined in [8] and [10]. The current expansion of Eq. (6) is inserted in the data equation of Eq. (3) and the boundary condition equation of Eq. (4)-(5). These coupled equations are finally solved by the iterative solution scheme described in [9], which allows one to achieve an accurate solution by balancing the effects of noise with the requirement of achieving Love's currents. It is noted that the higher order basis functions and higher order geometry modelling used by DIATOOL provide a smooth description of the currents and geometry relative to traditional RWG functions on flat triangular faces. The maximum dimension of the patches used by DIATOOL is two wavelengths. Since the size of traditional flat triangular patches lies typically in the range of lambda/100 and lambda/10, it is seen that DIATOOL requires a much smaller number of patches to describe the same reconstruction surface. This gives rise to a much faster computation time relative to formulations with RWG functions.

It is observed that the number of measured field samples sets an upper limit to the maximum number of unknowns that the 3D reconstruction algorithm can solve. In DIATOOL the maximum number of unknowns is approximately equal to twice the number of measurement samples. The number of unknowns depends on the number of patches used to mesh the closed surface, on which the currents are reconstructed.

Moreover, it depends on the accuracy of the polynomial expansion used to represent the unknown currents. The polynomial expansion order is automatically adapted to the electrical size of each patch, leading to the so-called "normal" accuracy. It can, however, be increased by an order at a time, by using "enhanced", "high" or "extreme" accuracy, if necessary. The "normal" and "enhanced" settings are in general sufficient when dealing with measured data with 70 dB SNR.

It is finally noted that, though it is recommended to use as large patches as possible, in order to limit the memory usage and the computation time, decreasing the patch dimension is sometimes advised, especially for array diagnostics, as it will be discussed in Section 3.

3. ARRAY DIAGNOSTICS

The identification of array element failure is of particular interest for antenna diagnostics, and mainly documented in the literature through experimental results, see for example [13]. Diagnostics of array failure, however, focuses often on results achieved by microwave holography, which is intrinsically limited in accuracy. Though noticeable improvements were recently achieved by [14], all proposed techniques assume the knowledge of the array element factor, either from a dedicated measurement or a software simulation. The capabilities of the 3D reconstruction algorithm on array diagnostics have not been studied in detail.

The 3D reconstruction of DIATOOL was applied to a 6 by 7 slotted waveguide array of dimensions 30 cm by 27 cm working at 5.25 GHz, with different row excitations and a conductive tape covering one slot, as shown in Figure 2. The antenna was measured at the DTU-ESA Spherical Near-Field Antenna Test Facility on a full sphere, with sampling in theta and phi equal to 2° and 4.5° respectively, and a SNR of 70 dB. The measurement coordinate system is shown in Figure 2: the origin coincides with the geometrical center of the array, the x-axis is horizontal, the y-axis is vertical and the z-axis points out of the paper. The distance between slots is 0.67 λ, with λ being the wavelength, along the vertical y-axis, and 0.85 λ along the horizontal x-axis. Since the product kr_o, where k is the wavenumber and r_o the radius of the antenna minimum sphere, is equal to 21, one finds that the Spherical Wave Expansion (SWE) of the field radiated by the antenna can be truncated to N=31, according to [12]. Once the maximum N is found, the sampling on the measurement sphere must at least be equal to

$$\Delta\theta = \Delta\varphi = \frac{180°}{N} \qquad (7)$$

which becomes $\Delta\theta=\Delta\varphi=5.8°$ for N=31. Consequently, the field measured at the DTU-ESA Facility has an oversampling factor of 2.9 in theta and 1.3 in phi,

relative to the value of 5.8°, and provides 7280 field samples distributed over the measurement sphere. This means that the maximum number of unknowns for the 3D reconstruction is approximately 14500.
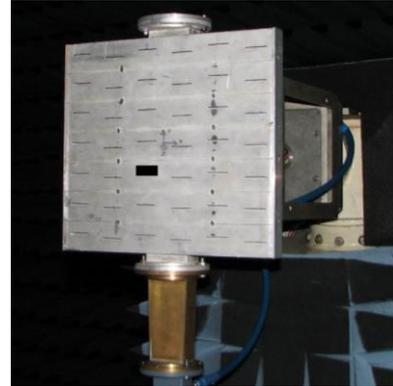

Figure 2 – The 6 by 7 slotted waveguide array in the DTU-ESA Spherical Near-Field Antenna Test Facility.

The reconstruction surface was a box conformal to the slotted waveguide array of Figure 2, with sizes 32 cm by 28 cm by 2 cm, with the top face coinciding with the array aperture. First, the maximum dimension of the patches was set to the default value of 2λ and the "enhanced" accuracy was chosen. This gave rise to 30 patches over the reconstruction box and 4536 unknowns. The computation time was 3.32 min on a laptop computer. The amplitude in dB of the y-component of the reconstructed tangential electric field on the top face of the box is shown in Figure 3, together with the used patches and the location of the covered slot.
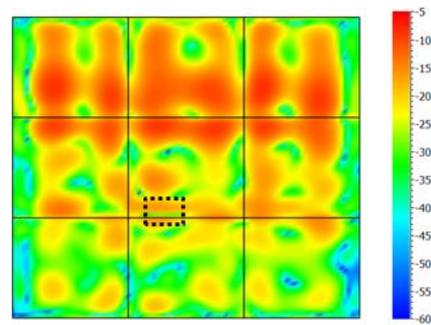

Figure 3 – Amplitude of the y-component of the tangential electric field from the 3D reconstruction, with patch size of 2λ and enhanced accuracy.

It is possible to distinguish the 6 by 7 slots; moreover, the radiation on the covered slot location looks different with respect to the rest of the aperture. The length of the patches was then reduced to 0.8λ, which almost coincided with the spacing of the slots along the horizontal axis, and gave rise to 142 patches over the

reconstruction box. By keeping the "enhanced" accuracy the number of unknowns became 8608. The computation time was 10 min on a laptop computer. The result of the reconstruction is shown in Figure 4. It is seen that the individual slots are better resolved when compared to Figure 3, both in the columns and rows, and that the covered slot is now clearly identified. Moreover, it can be observed that the slot rows 2 and 3 are strongly excited whereas rows 6 and 7 are very weak. This is in contradiction with the expected array excitation, which postulates a symmetric excitation relative to row 4, with row 4 being the one excited the most. This indicates that an error is present in the array feeding network. The result given by the traditional microwave holography on a plane of 32 cm by 28 cm located on the array aperture is shown in Figure 5. While the picture shows areas of high and low excitation similar to what is shown in Figure 3 and Figure 4, it is evident that the individual slots cannot be resolved, and that the resolution of the 3D reconstruction is far higher than the one provided by microwave holography.
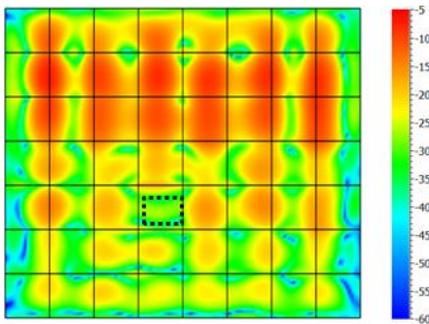

Figure 4 - Amplitude of the y-component of the tangential electric field from the 3D reconstruction, with patch size of 0.8 λ and enhanced accuracy.
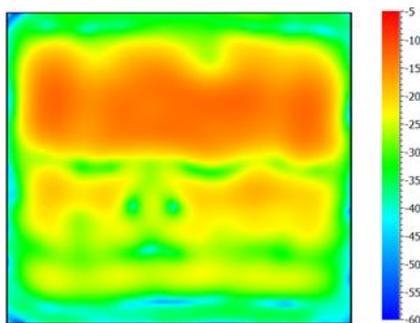

Figure 5 - Amplitude of the y-component of the tangential electric field from traditional microwave holography, i.e. invers Fourier transform of the far-field.

The effect of measured over sampling and the possibility of using truncated spherical data instead of full sphere data were studied in [15]. There it was shown that as long as full sphere data are available, the oversampling does not play a key role in the reconstruction. The use of truncated data, especially when combined with low oversampling has on the other hand a strong effect on the reconstructed field. It was shown that if the measured sphere was truncated to 82.8 deg and if the oversampling was 1.6, the reconstructed field looked very similar to the result provided by microwave holography, see Figure 5, and was very far from Figure 4.

3.1. Guidelines to achieve the best results

On the basis of the results presented in Section 3 and the considerations made there, we can conclude that the 3D reconstruction of DIATOOL provides the most accurate results for a slotted waveguide array if:

- Full sphere measurement data are used
- The measured field is slightly oversampled, i.e. a factor 2 in theta and 1.5 in phi should be sufficient
- The size of the patches is adjusted to almost coincide with the spacing of the array elements
- The expansion accuracy is the maximum allowed by the number of measured field points. "Enhanced" is thus recommended relative to "Normal", if the number of unknowns is manageable.

3.2. Achievable spatial resolution

Of fundamental importance for the quality and accuracy of a near-field plot is the concept of resolution. The word resolution is used in many different fields, and its definition can vary depending on the particular application. Generally resolution is the ability to distinguish the images of objects in close proximity.

In the field of holography and antenna diagnostics, resolution is defined by using the concept of plane wave expansion (PWE). Resolution is the distance between the zeros of the fastest oscillating wave contained in the PWE. If for example the fastest oscillating wave is given by $e^{ikx}=\cos kx + i \sin kx$ with k being the wave number, see Figure 6 (a) for a plot of the imaginary part, the obtainable resolution is equal to half a wavelength. This is also the distance that allows one to distinguish a positive amplitude from a negative amplitude. The definition can easily be extended to the two-dimensional case obtaining a resolution in the x- and one in the y- dimension.

Equivalently, resolution can be defined with the help of a concept always related to the PWE but more close to signal processing theory. Knowing that the spectral extent of a certain signal determines the spatial sampling necessary to reconstruct the original signal from its samples, according to $\Delta x = \pi / k_{max}$ for a one-dimensional signal with spectrum different from zero

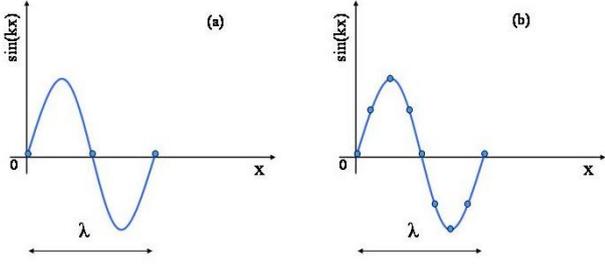over $[-k_{max}:k_{max}]$, resolution is then defined as the sampling interval Δx.

Figure 6 - Imaginary part of the wave e^{ikx}: (a) Resolution (b) Reconstruction interval from a zero-padded spectrum.

If $k_{max}=k$, we thus obtain a resolution of $\Delta x=\lambda/2$, like in the previous case. The interval Δx is also called reconstruction interval. It is pointed out that the sampling, or reconstruction, interval can be increased by zero-padding the available spectrum to a larger spectral domain, for example over the entire $[-4k:4k]$ domain. However, zero-padding does not increase at the same time resolution, since the spatial function obtained from the zero-padded spectrum is the same function of before, only oversampled, see Figure 6 (b). As long as the spectrum is different from zero over the only $[-k:k]$ domain, resolution remains equal to half a wavelength. Resolution is thus only determined by the part of the plane wave spectrum which is different from zero. The presence of noise does not directly influence the resolution with this definition. If the field is computed as inverse Fourier transform of the far-field, resolution remains half a wavelength no matter if the far-field is noisy or noiseless, since the invisible region of the PWS will always be disregarded. If the plane wave spectrum is not obtained from the far-field, but from the SWE-to-PWE transformation [2], noise-free data will allow the recovery of part of the invisible region and thus provide a resolution higher than half a wavelength. For noisy data with SNR=60 dB, the invisible region will most probably be ignored and thus the resolution will be half a wavelength.

From the definitions above, we conclude that the resolution given by microwave holography, i.e. by inverse Fourier transforming the far-field, is half a wavelength. It turns out however, that in practice sources located half a wavelength apart cannot be distinguished by microwave holography, see [16]. To show this, we consider an array of three y-oriented Hertzian dipoles located on the xy-plane and displaced by a distance d that varies from 2λ to 0.5λ. The electric field on the $z=0.1\lambda$ plane is computed. When the PWS is non-zero only on the visible region, though resolution is in principle equal to $\lambda/2$, the three dipoles are clearly distinguished only for $d=2\lambda$. For $d=\lambda$ the sources are distinguished on the horizontal axis, but not on the

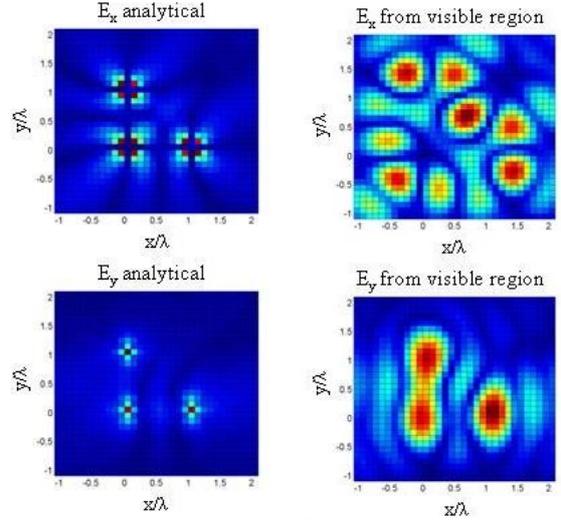vertical axis, see Figure 7, while for $d=\lambda/2$ the dipoles cannot be resolved at all, see Figure 8.

Figure 7 - Amplitude of x- and y-component of the tangential electric field on the $z=0.1\lambda$ plane from three y-oriented Hertzian dipoles separated by $d=\lambda$.

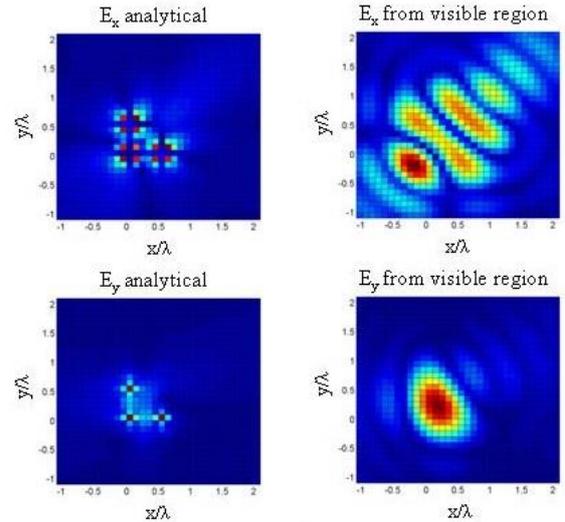*Figure 8 - Amplitude of x- and y-component of the tangential electric field on the $z=0.1\lambda$ plane from three y-oriented Hertzian dipoles separated by $d=\lambda/2$.*

It is noted that the three dipoles are however better distinguished in the y-component than in the x-component. It is also recalled that the dipoles can be resolved up to $d=\lambda/2$ if the spectrum is known in the invisible region in the entire domain $[-5k:5k]$. This leads us to the conclusion that resolution perceived by the human eye in observing a near-field plot cannot be defined by a specific formula and it might be lower than the expected one, since even at very short distances from the aperture the electromagnetic field is not a point function but has a spatial extent. While the perception of the eye can be improved by choosing between a dB

scale or a linear scale, and by properly setting the color scale in order to highlight certain differences and increase the contrast, the nature of the electromagnetic field radiated by the sources influences what the eye perceives. In particular it was noted that what the eye distinguishes generally depends on the polarization of the source, the plane of interest, and the component of the field.

With this background, it is important to recall that the 3D reconstruction of DIATOOL has no hard limit on the resolution of the reconstructed currents. To this end, the example shown in [8] is reported in Figure 9.
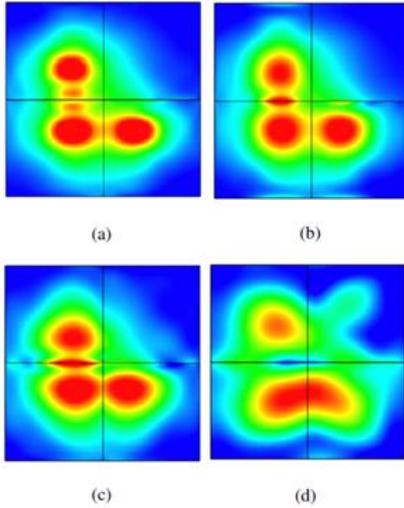

(a)   (b)

(c)   (d)

Figure 9 – Electric field on the z=0.1 λ plane from three Huygens sources separated by λ/4: (a) reference field, (b) the best possible field for the present discretization (MoM), (c) field reconstructed from far-field data without noise, (d) field reconstructed from far-field data with SNR=60 dB.

The figure shows the electric field of three Huygens sources located on the *xy*-plane and separated by a distance of λ/4. The field is computed on the *z*=0.1λ plane. In the noise less condition, the field can be reconstructed nearly without loss of information: the sources are distinguished, though small artefacts may occur. For noisy data, sources separated by λ/4 may or may not be distinguished, depending on the direction.

We can conclude therefore that the resolution of the 3D reconstruction from noise-free far-field data is higher than the one of microwave holography from far-field data, i.e. the 3D reconstruction can distinguish sources that are not distinguishable by microwave holography. The reason for this difference in resolution is due to the fact that the 3D reconstruction considers in its formulation the a-priori information that sources are confined inside the reconstruction surface, while microwave holography does not. The reconstruction surface conformal to the antenna becomes a physics-based filter. This explains the difference in the results

obtained in Figure 4 and Figure 5 for the slotted waveguide array.

On the other hand, the resolution of the 3D reconstruction from noise-free far-field data can be comparable to the one given by the SWE-to-PWE transformation of a noise-free far-field.

To fully appreciate the capabilities of the 3D reconstruction, two more observations need to be made. The currents reconstructed by the 3D reconstruction of DIATOOL provide a field which is noise-free, see Figure 10, where the SWE of the measured field of the slotted waveguide array of Figure 2 is compared to the SWE of the field radiated by the reconstructed currents of Figure 4. It is seen that the electrical noise floor at -60 dB is removed and substituted by a numerical noise floor at -120 dB.
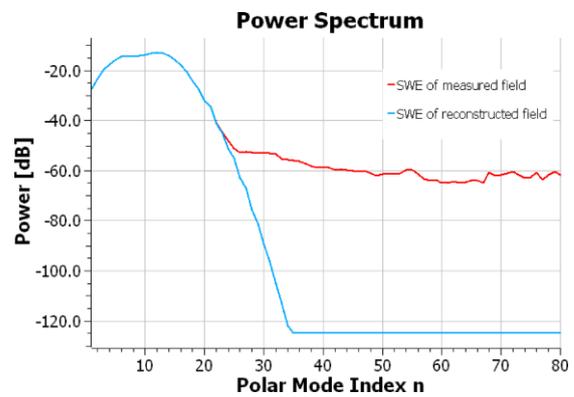

Figure 10 – Power spectrum of SWE of the measured field of the slotted waveguide array of and of the SWE of the field radiated by the reconstructed currents of Figure 4.

The noise-free SWE of the reconstructed field, i.e. the blue curve of Figure 4, can be used as input to DIATOOL to reconstruct with the planar reconstruction the field over a plane coinciding with the top face of the slotted waveguide array. The SWE of the measured field did not allow recovering the invisible region of the plane wave spectrum, and produced the result reported in Figure 5. The SWE of the reconstructed field allows recovering part of the invisible region and produces the result of Figure 11. By comparing Figure 11 with Figure 5 we see that the resolution has improved in the horizontal direction, since now the six columns are visible. In the horizontal direction the improvement is smaller. On the other hand, Figure 4 is still better than Figure 11. As last observation it is worth repeating, as shown in Section 3, that the 3D reconstruction of DIATOOL allows one to adjust the maximum length of the patches to let that coincide with the spacing of the array, and producing therefore more accurate field results.
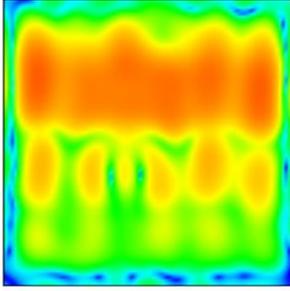
Figure 11 - Amplitude of the y-component of the tangential electric field obtained by the planar reconstruction of DIATOOL from the SWE of the field reconstructed by the 3D reconstruction.

4. FILTERING OF UNDESIRED RADIATION

The last important feature of the 3D reconstruction algorithm of DIATOOL is the ability of identifying the undesired sources of radiation and scattering, such as for example leaking cables and antenna support structures, which can affect the performances of the antenna. Of particular interest is the subsequent filtering of this undesired radiation, to obtain a more accurate measured field.

An example of this application is reported in the following. The 7 by 8 patch array of Figure 12 was measured at the DTU-ESA Spherical Near-Field Antenna Test Facility on a full sphere, with sampling in theta and phi equal to 3° and 5° respectively. The size of the patch array was 30 cm by 36 cm and the frequency 5.3 GHz. The 3D reconstruction of DIATOOL was applied on a box of 30 cm by 36 cm by 0.8 cm with a mesh of 0.8λ size and the "enhanced" expansion accuracy, as it was done in Section 3 for the slotted array.

Figure 12 – The 7 by 8 patch array.

The obtained *x*-component of the electric field on the top face of the box is shown in Figure 13 on the left. It is observed that the result almost coincides with the one obtained by traditional microwave holography, shown in Figure 13 on the right. The patches cannot be resolved, like in Figure 4. This is probably due to the

fact that slots are more localized sources than patches. The figure shows that the excitation of the patch arrays is symmetric relative to a vertical axis passing for the centre. Moreover, a defective patch can be identified.
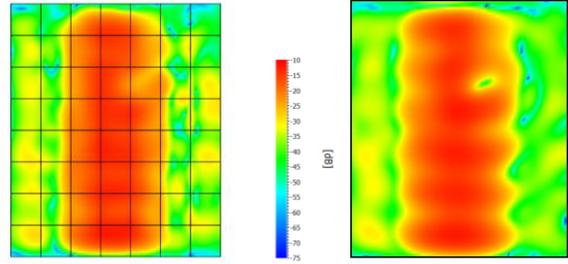

Figure 13 – Amplitude of the x-component of the electric field: on the left the result from the 3D reconstruction, on the right from microwave holography.

The 3D reconstruction reported however a very poor match with the measured data, meaning that some sources were located outside the reconstruction surface. It was therefore decided to enclose the back structure in the reconstruction surface, according to Figure 14, and rerun. The match with the measured data set improved by 20 dB and reached an acceptable value.
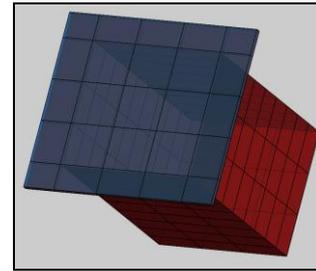

Figure 14 – New reconstruction surface enclosing both the patch array and the backing structure.

The obtained currents showed, see Figure 15, that strong currents originating from the radiation of the feed network were present on the back structure.
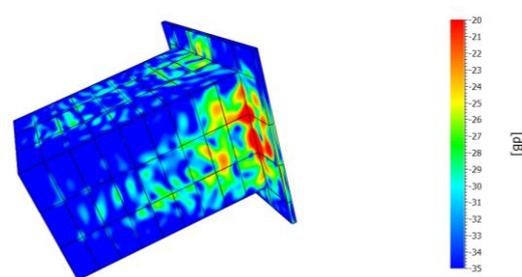

Figure 15 – Amplitude of total electric currents reconstructed by DIATOOL.

Later on, the currents on the back structure were imposed as non-radiating and the field radiated only by the currents on the top box were computed and compared with the field measured at the DTU-ESA

facility, see Figure 16. The effect of the leaking feeding network was thus removed.
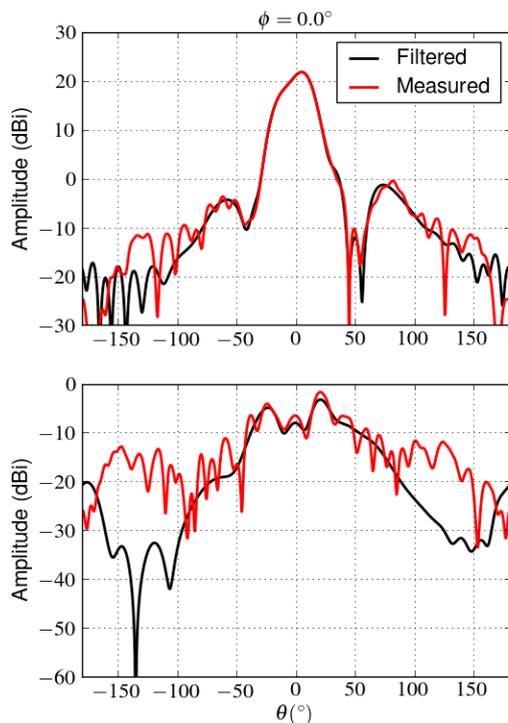

Figure 16 – Amplitude of the co-polar and cross-polar components of the patch array measured field and the field radiated by the currents on the top box, when the unwanted radiation from the feeding network is disregarded.

5. CONCLUSIONS

The accuracy and capabilities of the 3D reconstruction algorithm of DIATOOL were presented, relative to array diagnostics, obtainable spatial resolution and filtering of undesired radiation. It was shown that all the 6 by 7 slotted waveguides could be resolved, if full sphere data were used and if the size of the patches forming the reconstruction surface was adjusted to almost coincide with the spacing of the array elements. The spatial resolution achievable by the 3D reconstruction of DIATOOL was studied and compared with the results obtainable by traditional microwave holography: the resolution of the 3D reconstruction from noise-free far-field data is higher than the one of microwave holography from far-field data, since the 3D reconstruction considers the a-priori information that sources are confined inside the reconstruction surface, Finally, an example of filtering of undesired on a patched array was shown.

REFERENCES

[1] H. G. Booker, P. C. Clemmow, "The concept of angular spectrum of plane waves and its relation to that of polar diagram and aperture distribution", Proc. Inst. Elec. Eng., vol. 97(1), pp. 11-16, January 1950.

[2] C. Cappellin, O. Breinbjerg, A. Frandsen, "Properties of the transformation from the spherical wave expansion to the plane wave expansion", Radio Science, vol. 43, no. RS1012, doi:10.1029/2007RS003696, February 2008.

[3] T. K. Sarkar, A. Taaghol, "Near-field to near/far-field transformation for arbitrary near-field geometry utilizing and equivalent electric current and MoM," IEEE Trans. Antennas Propagat., vol. 47, no. 3, pp. 566–573, Mar. 1999.

[4] Y. Alvarez, F. Las-Heras, M. R. Pino, "Reconstruction of equivalent currents distribution over arbitrary three-dimensional surfaces based on integral equation algorithms", IEEE Trans. Antennas Propagat., vol. 55, no. 12, pp. 3460–3468, Dec. 2007.

[5] T. F. Eibert, C. H. Schmidt, "Multilevel fast multipole accelerated inverse equivalent current method employing Rao-Wilton-Glisson discretization of electric and magnetic surface currents", IEEE Trans. on Antennas Propag., vol. 57, no. 4, pp. 1178–1185, 2009.

[6] J. L. A. Quijano, G. Vecchi, "Improved-accuracy source reconstruction on arbitrary 3-D surfaces", IEEE Antennas and Wireless Propagation Letters, vol. 8, pp. 1046–1049, 2009.

[7] K. Persson and M. Gustafsson, "Reconstruction of equivalent currents using a near-field data transformation - with radome applications", Progress in Electromagnetics Research, vol. 54, pp. 179–198, 2005.

[8] E. Jørgensen, P. Meincke, C. Cappellin, and M. Sabbadini, "Improved source reconstruction technique for antenna diagnostics", Proc. of the 32nd ESA Antenna Workshop, ESTEC, Noordwijk, The Netherlands, 2010.

[9] E. Jørgensen, P. Meincke, O. Borries, and M. Sabbadini, "Processing of measured fields using advanced inverse method of moments algorithm", Proc. of the 33rd ESA Antenna Workshop, ESTEC, Noordwijk, The Netherlands, 2011.

[10] E. Jørgensen, J. L. Volakis, P. Meincke, and O. Breinbjerg, "Higher order hierarchical Legendre basis functions for electromagnetic modelling", IEEE Trans. Antennas Propagat., vol. 52, no. 11, pp. 2985–2995, Nov. 2004.

[12] F. Jensen, A. Frandsen, "On the number of modes in spherical wave expansions", Proc. Antenna Meas. Tech. Ass. Symposium, AMTA 2004, pp. 489-494, 2004.

[13] J. J. Lee, E. M. Ferren, D. P. Woollen, K. M. Lee, "Near-field probe used as a diagnostic tool to locate defective elements in an array antenna", IEEE Trans. Ant. Prop., vol. 36, no. 6, June 1988.

[14] D. W. Hess, S. T. McBride, "Imaging of element excitations with spherical scanning", Proc. Antenna Meas. Tech. Ass. Symposium, AMTA 2011, pp. 329-334, 2011.

[15] C. Cappellin, P. Meincke, E. Jørgensen, "Array antenna diagnostics with the 3D reconstruction algorithm", Proc. of AMTA conference, Bellevue, Washington, October 2012.

[16] C. Cappellin, "Antenna diagnostics for spherical near-field antenna measureemnts", Ph. D. thesis, Electromagnetic Systems, Department of Electrical Engineering, Technical University of Denmark, 2800, Kgs. Lyngby, January 2008.